Patient-specific stress/strain calculations in the tissues

Project Number: FP7--IST-*223979*
Deliverable id: D6.2
Deliverable name: Patient-specific stress/strain calculations in the tissues
Submission Date: 30/04/2010

COVER AND CONTROL PAGE OF DOCUMENT

Project Acronym:	CONTRA CANCRUM
Project Full Name:	Clinically Oriented Translational Cancer Multilevel Modelling
Document id:	D6.2
Document name:	Patient specific stress/strain calculations in the tissues
Document type (PU, INT, RE)	RE
Version:	1
Submission date:	31/04/2010
Editor: Organisation: Email:	Thibaut Bardyn, Philippe Büchler UNIBE thibaut.bardyn@istb.unibe.ch

Document type PU = public, INT = internal, RE = restricted

ABSTRACT:
D6.2 Patient-specific stress/strain calculations in the tissues, Report on the calculation of the mechanical environment in the brain and lung during tumor growth for the simulation of cancer biomechanics. Final version delivered in end of April 2010, after early drafts circulated within consortium...

KEYWORD LIST: finite element, patient-specific, stress, strains

MODIFICATION CONTROL			
Version	Date	Status	Author
1.0	30/04/10	Template	Thibaut Bardyn

List of Contributors

- Thibaut Bardyn, University of Bern
- Philippe Büchler, University of Bern

Contents

Executive Summary

The ContraCancrum, i.e. the Clinically Oriented Translational Cancer Multilevel Modelling, project aims at developing a composite multilevel platform for simulating malignant tumour development and tumour and normal tissue response to therapeutic modalities and treatment schedules.

The project aims at having an impact primarily in (a) a better understanding of the natural phenomenon of cancer at different levels of biocomplexity and, most importantly, (b) a disease treatment optimization procedure in the patient's individualized context by simulating the response to various therapeutic regimens. The predictions of the simulators to be developed will rely on the imaging, histopathological, molecular and clinical data of the patient. Fundamental biological mechanisms involved in tumor development and tumor and normal tissue treatment response such as metabolism, cell cycle, tissue mechanics, cell survival following treatment etc. will be modeled. Stem cells will be addressed in the context of both tumor and normal tissue behavior. From a mathematical point of view, the simulators will exploit several discrete and continuous mathematics methods such as cellular automata, the generic Monte Carlo technique, finite elements, differential equations, novel dedicated algorithms etc. A study of the analogies of tumor growth with embryological development is expected to provide insights into both mechanisms.

ContraCancrum will deploy two important clinical studies for validating the models, one on lung cancer and one on gliomas. The crucial validation work will be based on comparing the multi-level therapy simulation predictions with the actual medical data (including medical images), acquired before and after therapy.

ContraCancrum aims to pave the way for translating clinically validated multilevel cancer models into clinical practice.

This deliverable presents the calculation of the mechanical constraints in the tissue due to tumor growth. Examples are shown for both models of brain and lung generated by the algorithm presented in the D6.1. The calculations are performed with an open source software modified for the purpose of the Oncosimulator. To take the simulation further a coupled approach combining diffusion/reaction and mass effect of the tumor is also presented.

The innovative oncosimulator that will be developed in the framework of the Contra Cancrum European project combines a biomechanical and a cellular model. The biomechanical simulation aims at calculating the mechanical state in the anatomy around the tumor during its growth. This mechanical information is then transferred to the cellular simulator which will predict the behavior of the cells within this tumor.
The following report presents the calculation of the mechanical information that will be provided to the cellular model. FEBio, an open source code that offers more flexibility as compared to existing commercial software, is used for that purpose.

1 Scientific background and previous work

1.1 Biomechanical models of the brain

Biomechanical model of the brain and head in general were primarily used for the study of trauma in traffic accidents (Voo et al., 1996). Similarly, these finite element models were also used to explain impact in the head in forensic practice (Raul et al., 2008). This domain has been extended to clinical applications such as image-guided neurosurgery. In this technology, models are used to simulate deformation of brain (or brain shift) that might impair registration of the images to the patient (Carter et al., 2005; Wittek et al., 2007).
For the majority of models, small deformations and material linearity are assumed. The reason for this is twofold. First it allows a fast solution of the model. Second, the experimental data on brain tissue for surgery is extremely scarce. The majority of the investigation work has been done for traumatic injury and thus at strain rates larger than those for surgery. Poroelastic (Taylor & Miller, 2004) and non-linear viscoelastic (Miller, 1999) models were progressively introduced but the question remains whether the increased complexity of these models results in a significantly improvement in accuracy.
Tetrahedral and hexahedral elements have been equally used for these models. However, hexahedral elements seem to be more adapted because they offer better performances with incompressible material such as the cerebrospinal fluid (CSF).

1.2 Biomechanical models of the lung and chest

Similarly to brain models, lung and chest models found their first occurrence in simulation of injury in car crashes. Later, finite element models have also been used to simulate physiological phenomena in the lung such as air flow in the conducting airways (van Ertbruggen et al., 2005), gas exchange in the parenchyma (Cookson et al., 1993) and breathing pathologies (Sundaram & Gee, 2005).
Mechanical properties of the lung have been retrieved using different methods. Pressure and volume change in the lung were measured using specific devices and related to find the tissue macroscopic properties (Bates, 1993). In another methodology, four-dimensional CT images have also been used. A finite element model is built and the properties of the lung material are optimized so to match the movement of the lung structures during breathing on these images (Al Mayah et al., 2009). Finally, biaxial tests have been performed on the tissue

itself (Zeng et al., 1987). For relatively small and quasi static deformations, non invasive measurements based on volume and pressure have shown that the lung is a linear elastic material (Bates, 1993). For larger deformation, an exponential law is commonly used in models (Zeng et al., 1987; Tawhai et al., 2009).

1.3 Biomechanical model of tumor growth

Finite element simulation of tumor growth has been used to aid the registration of brain tumor images. The brain atlas used for the registration is modified so to improve matching with the patient image. In these models, growing of the tumor is modeled as an outward pressure acting on the tumor boundary (Mohamed & Davatzikos, 2005). However, the aim of these models is merely to match the actual shape of the tumor in the image and therefore they only consider the mass effect of tumor growth and do not have predictive values. Predicting the tumor behavior implies the addition of a diffusion/reaction model in the simulation. Unlike most cancerous cells which primarily grow, gliomas for example are highly diffusive (Murray, 2003; Swanson, 1999). For this reason, numerous studies have been perfomed that simulate tumor growth as a pure diffusion/reaction phenomenon without considering the mechanical aspect and the deformation of tissue (Chakrabarty & Hanson, 2009; Swanson, 1999). Wassermann et al. (Wasserman & Acharya, 1996) and later Clatz et al. (Clatz et al., 2004) have introduced simulations that combines physiological effect such as diffusion and mechanical growth. These models allow the prediction of the deformation for the surrounding tissues after a certain time. The future of such models lies now in the characterization of physiological parameters which will improve their accuracy (Konukoglu et al., 2007). Indeed, one of the main limitations to this model is the lack of patient-specific information (Juffer et al., 2008).

1.4 FEBio

This section presents the open source code that is used for the calculation of stresses and strains in the tissue. The software has been compared with commercial finite element products in terms of speed and accuracy.

1.4.1 General description

FEBio is an open source software that uses the finite element method for solving nonlinear large deformation problems in solid biomechanics. It is specifically aimed at solving problems in the field of biomechanics, by providing appropriate modeling scenarios, constitutive models and boundary conditions. It has been developed by Steve Maas from the University of Utah under the supervision of Jeff Weiss. FEBio has been chosen for the ContraCancrum project for several reasons:

- It is open source and therefore allows implementation of specific processes such as tumour growth or reaction/diffusion.
- It includes non linear finite element and complex physiological material properties. This is particularly useful when modeling living tissues such as the brain or the lung.
- The support provided by the University of Utah is particularly efficient and questions are answered in a short time.
- It is being used by an increasing number of universities and research labs, making the FEBio community particularly active

However, for the purpose of this project, FEBio has several limitations that need to be overcome. The main limitation is the absence of thermal expansion laws and thermal/mechanical coupling needed for the simulation of tumor growth. This had therefore to be added to the original code. Another limitation is the basic graphic user interface that does not allow easy verification of the models. The meshes used in the following report were verified using the commercial software ABAQUS. This does not jeopardize the use of FEBio in the oncosimulator since only the command line will be used.
For the solution of the problems presented in the rest of the report, the Pardiso solver is used. The PARDISO solver is a thread-safe, high-performance, robust, memory efficient and easy to use software for solving large sparse symmetric and unsymmetric linear systems of equations on shared memory multiprocessors. The solver has been licensed to thousands of researchers at international scientific laboratories and universities since its first release in 2004.

1.4.2 Evaluation of performance

The evaluation of FEBio performance was done by comparing its speed and results again ABAQUS. The comparison was performed on one of the benchmark simulations provided with the FEBio package (Maas et al., 2009). This simulation was chosen because it illustrated concept used in the future for the Oncosimulator such as living tissue material properties.
The problem considered was the compression of a billet of material between two flat surfaces (figure 1). Two cases were simulated. First the flat surfaces were not considered and the compression was done by applying a displacement constraint to the nodes on the top surface of the billet (non contact case). Second, two rigid surfaces were used for the compression and a frictionless contact was defined between these surfaces and the billet (contact case). Because of the symmetry of the problem, only a quarter of the billet was simulated. The billet was defined as a non linear material following a Neo Hookean law:

$$W = C_1(I_1 - 3) + D_1(J-1)^2; \mathrm{J} = \det(\mathrm{F})$$

With W the strain energy density, I_1 the first invariant of the left Cauchy-Green deformation tensor, and **F** the deformation gradient. This type of material law is typically used to simulate rubber-like substances. It is also frequently chosen to simulate soft tissues. For the present

simulations, C_1 was set to 0.16 while D_1 was equal to 0.12 corresponding to a nearly incompressible material having a Young's modulus of 1. Again, incompressible assumptions are commonly used in biomechanical simulation (for the CSF in the brain for example). The compression was done up to 20% of the billet height for the non contact case and up to 50% for the contact case. The horizontal displacement of the top right node of the mesh (the billet bulge) was plotted versus the percent compression.

Results showed a good match between FEBio and ABAQUS both for the non contact and the contact case (figure 2). In terms of speed, the simulation time was equivalent for both ABAQUS and FEBio on a Intel Core 2, 2GHz with 1G of RAM (table 1). The difference in time for the contact case is probably due to a difference in the formulation in contact for the two software leading to a different convergence speed.

In parallel to the present example, many other tests have been conducted to assess the speed and accuracy of FEBio as compared to other products. These confirm the validity of this tool and the fact that it can be used for clinical applications such as the Oncosimulator of the ContraCancrum project.

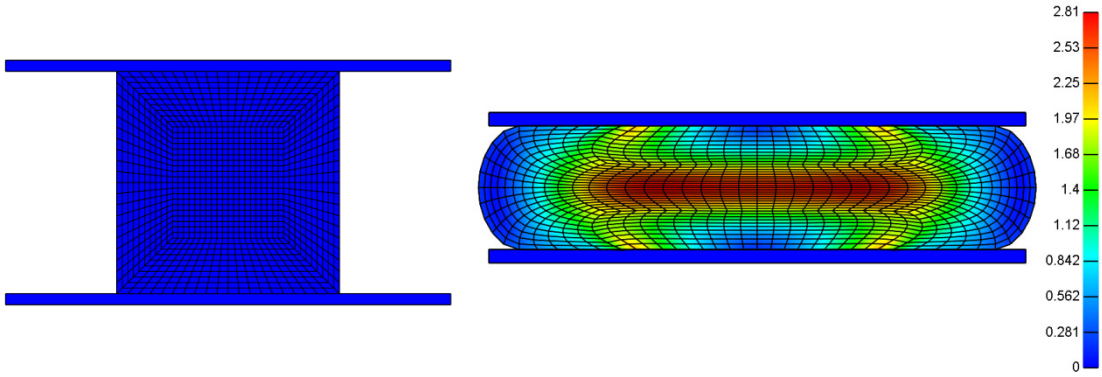

Figure 1: (left) Undeformed configuration of the billet simulation with shape enclosed between the two sufaces (right) Deformed configuration with a 50% deformation showing the Mises stresses.

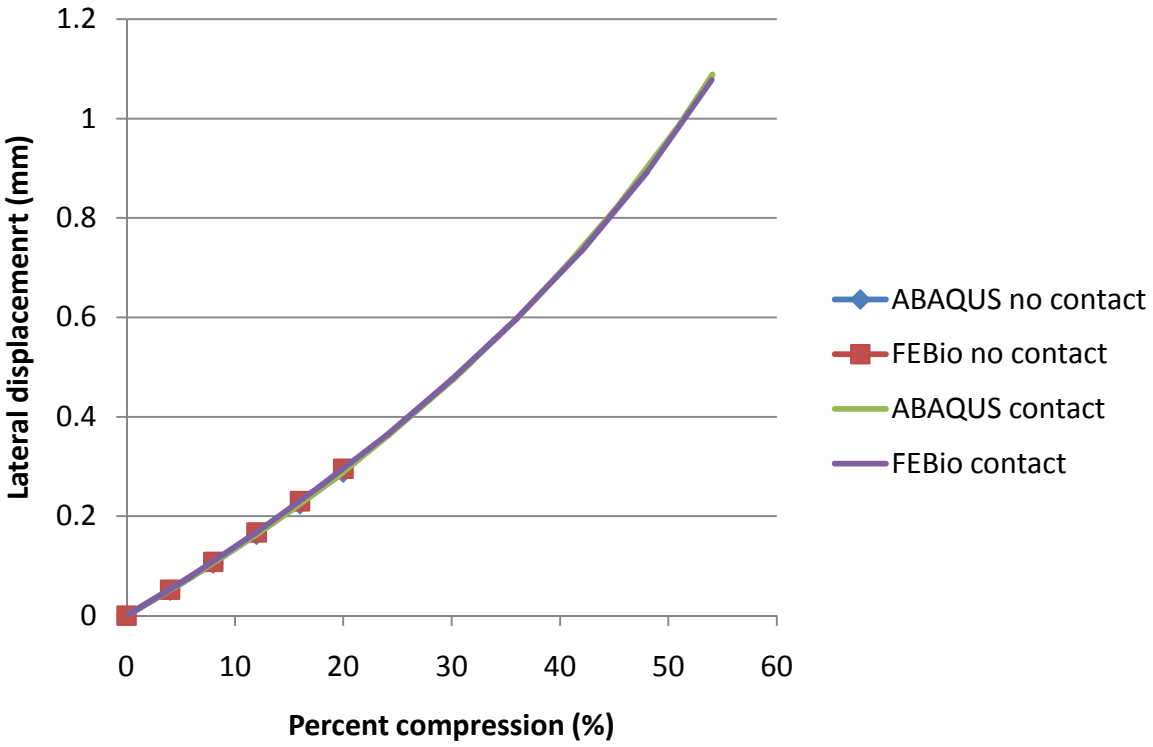

Figure 2: Lateral displacement of the billet versus the percent compression as calculated by FEBio and ABAQUS for the contact and non contact case.

	FEBio (s)	ABAQUS (s)
No contact	2	4.9
contact	15	13.4

Table 1: Simulation time for FEBio and ABAQUS for the non contact and contact case.

2 Simulation of tumor growth

This section introduces the material law that was used for the simulation of the mass effect in tumor growth. The law is based on the theory of finite elasticity.

2.1 General principle

Before the material law for the mass effect is introduced, a few facts on finite elasticity need to be defined. The work done by external forces in deforming an elastic body is stored within the body in the form of strain energy. The simplest hyperelastic model is the Kirchoff-St

Venant model, which can be used for large displacements where the material undergoes small strains. The strain-energy density function for this model is given by:

$$W = \frac{\lambda}{2} Trace(\mathbf{E})^2 + \mu Trace(\mathbf{E}^2)$$

With **E** the Lagrange-Green strain tensor. λ, μ are the Lamé constants that represent the mechanical properties of the material. They are related to the Young's modulus *E* and Poisson ratio *v* by the formula:

$$\lambda = \frac{\nu E}{(1+\nu)(1-2\nu)}, \mu = \frac{E}{2(1+\nu)}$$

When in an isotropic linear elastic solid, the stress vector, given as $\mathbf{S} = \frac{\partial W}{\partial \mathbf{E}}$, is defined by the Hook's law:

$$\mathbf{S} = \lambda Trace(\mathbf{E})\mathbf{I} + 2\mu\mathbf{E}$$

The stress/strain relationship can be written in the form of a matrix relation, giving:

$$\begin{pmatrix} \mathbf{S}_{XX} \\ \mathbf{S}_{YY} \\ \mathbf{S}_{ZZ} \\ \mathbf{S}_{XY} \\ \mathbf{S}_{YZ} \\ \mathbf{S}_{XZ} \end{pmatrix} = \frac{E}{(1+\nu)(1-2\nu)} \begin{pmatrix} 1-\nu & \nu & \nu & 0 & 0 & 0 \\ \nu & 1-\nu & \nu & 0 & 0 & 0 \\ \nu & \nu & 1-\nu & 0 & 0 & 0 \\ 0 & 0 & 0 & \frac{(1-2\nu)}{2} & 0 & 0 \\ 0 & 0 & 0 & 0 & \frac{(1-2\nu)}{2} & 0 \\ 0 & 0 & 0 & 0 & 0 & \frac{(1-2\nu)}{2} \end{pmatrix} \begin{pmatrix} \mathbf{E}_{XX} \\ \mathbf{E}_{YY} \\ \mathbf{E}_{ZZ} \\ 2\mathbf{E}_{XY} \\ 2\mathbf{E}_{YZ} \\ 2\mathbf{E}_{XZ} \end{pmatrix}$$

With $\mathbf{E}_{XX}$, $\mathbf{E}_{YY}$, $\mathbf{E}_{ZZ}$ the three components of the strains in the main directions and $\mathbf{E}_{XY}$, $\mathbf{E}_{YZ}$, $\mathbf{E}_{XZ}$ the three shear components; $\mathbf{S}_{XX}$, $\mathbf{S}_{YY}$, $\mathbf{S}_{ZZ}$, $\mathbf{S}_{XY}$, $\mathbf{S}_{YZ}$, $\mathbf{S}_{XZ}$ the six components of the stress vector.

The growth was considered as isotropic and uniform. The change in volume was modeled as a uniform strain added in the three main directions in the elastic formulation of the element.

$$\mathbf{E} = \mathbf{E}_{MECH} - \mathbf{E}_{GROWTH}$$

With $\mathbf{E}_{MECH}$ and $\mathbf{E}_{GROWTH}$ the mechanical and added growth component of the strain vector respectively. This can be interpreted as a tissue internal pressure. To simulate the mass effect of tumor, the mechanical equations were modified as follows. The trace of the strain tensor became:

$$Trace\ \mathbf{E} = \mathbf{E}_{XX} + \mathbf{E}_{YY} + \mathbf{E}_{ZZ} - (3*\mathbf{E}_{GROWTH})$$

The constitutive equations given by the strain energy function were then changed to:

$$\mathbf{S}_{XX} = \lambda * tr\mathbf{E} + 2*\mu*(\mathbf{E}_{XX} - \mathbf{E}_{growth})$$
$$\mathbf{S}_{YY} = \lambda * tr\mathbf{E} + 2*\mu*(\mathbf{E}_{YY} - \mathbf{E}_{growth})$$
$$\mathbf{S}_{ZZ} = \lambda * tr\mathbf{E} + 2*\mu*(\mathbf{E}_{ZZ} - \mathbf{E}_{growth})$$
$$\mathbf{S}_{XY} = 2*\mu*(E_{XY})$$
$$\mathbf{S}_{YZ} = 2*\mu*(E_{YZ})$$
$$\mathbf{S}_{XZ} = 2*\mu*(E_{XZ})$$

A new material was created in FEBio that calculated the stress in the element according to the equations presented. This material took as arguments the Young's modulus, Poisson ratio and constant growth factor $\mathbf{E}_{GROWTH}$. The main advantage of this approach is its flexibility. It can easily be adapted to complex and physiologically valid strain energy functions/constitutive models.

2.2 Test case

The method was tested on a geometrical example. A 10mm radius sphere (representing the tumor) was embedded in a 50mm radius one (representing the surrounding tissue). Both external and internal sphere were assumed to have the same mechanical properties with a Young's modulus of 1000 and a Poisson ratio of 0.3. A growth strain of 10% was considered.
Results showed a uniform growth of the tumor (figure 3). The volume increase due to the strain was about 18%. This corresponds to an increase in radius of 4.1%. The real increase in radius is smaller than the increase in strain because of external constraint generated by the surrounding tissue. This approach allows to apprehend the interaction of the tissue on the tumor.

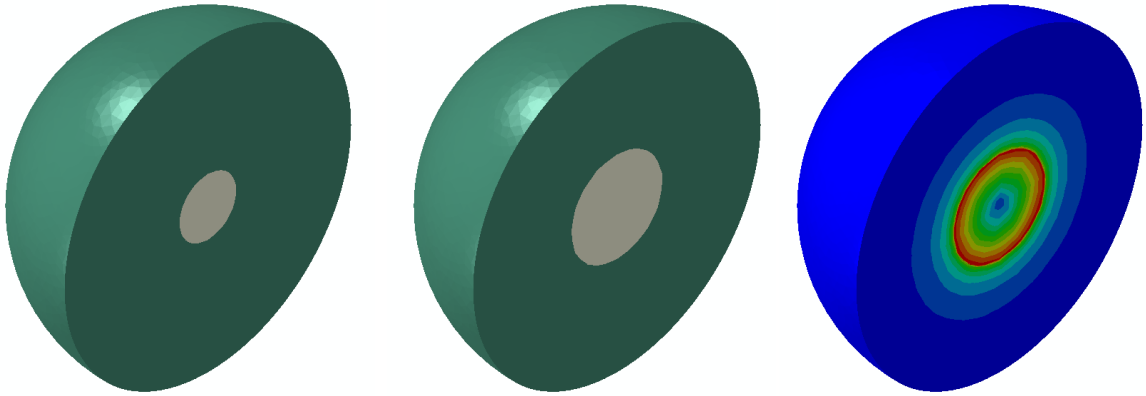

Figure 3: Sphere example for the growth material law (left to right) undeformed model, deformed model with larger inner sphere, deformed model with displacement field

3 Calculation of stresses and strains in the brain

This section presents the construction of a generic brain model as well as the calculation of the stresses and strains due to the tumor growth via finite element analysis.

3.1 Brain images

The SRI24 Atlas (Rohlfing et al., 2010) was used as a basis to generate the model. This atlas represents the brain anatomy of a normal adult and contains 240x240x155 voxels. It is used as an atlas by the WP7 for the segmentation of brain images. This phantom also includes a labeled version with segmented structures. The following anatomical areas are isolated:

- White matter
- Grey matter
- Cerebrospinal fluid

A tumor was artificially added to the mask using a custom ITK script. It was represented by a 10mm radius sphere (figure 4) and placed in a zone such as to be in contact with different structures. The same type of model was used by the WP7 to initialize the tumor deformation used for the segmentation.

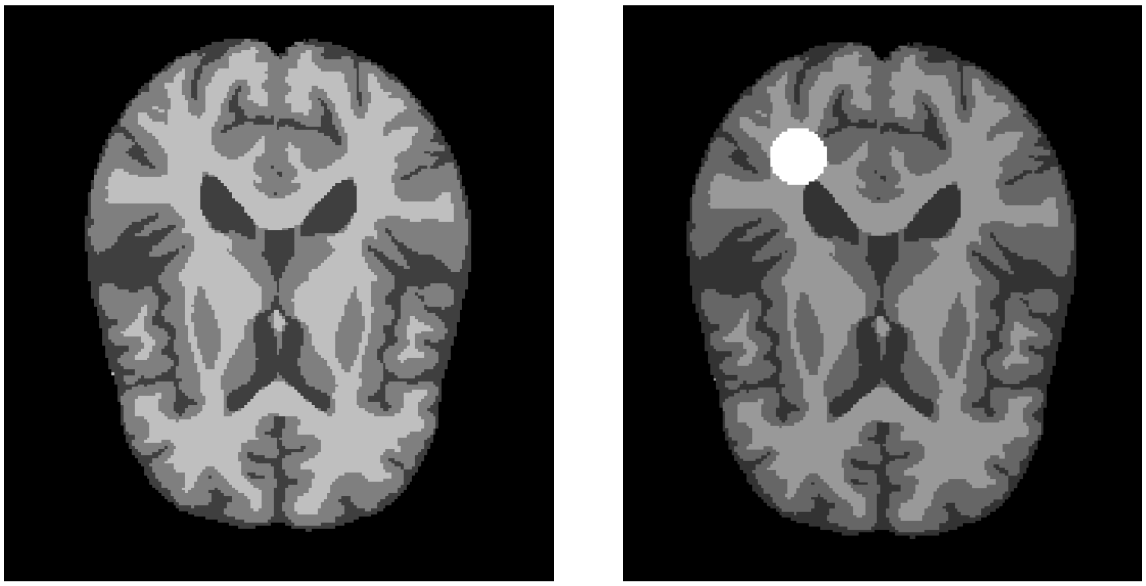

Figure 4: (left) The segmented SRI24 brain atlas used for the generation of the model. It contains three labels. (right) the phantom with the artificial tumour added.

3.2 Generation of the finite element mesh

A finite element model of the brain was generated using the automatic smooth mesh generator presented in the D6.1. This algorithm generates a cubic element mesh that is then smoothed. For the brain model, a smoothing factor of k=0.03 was used since it was found to give the most optimal trend between quality of element and accuracy (see D6.1). The quality of elements was improved by using the division of deformed hexahedron elements into prism elements. If elements with negative jacobians were left after prism correction, they were removed from the mesh. The whole process (including the assignment of material properties) was entirely automatic. The model could be fed into the finite element solver immediately after this step.

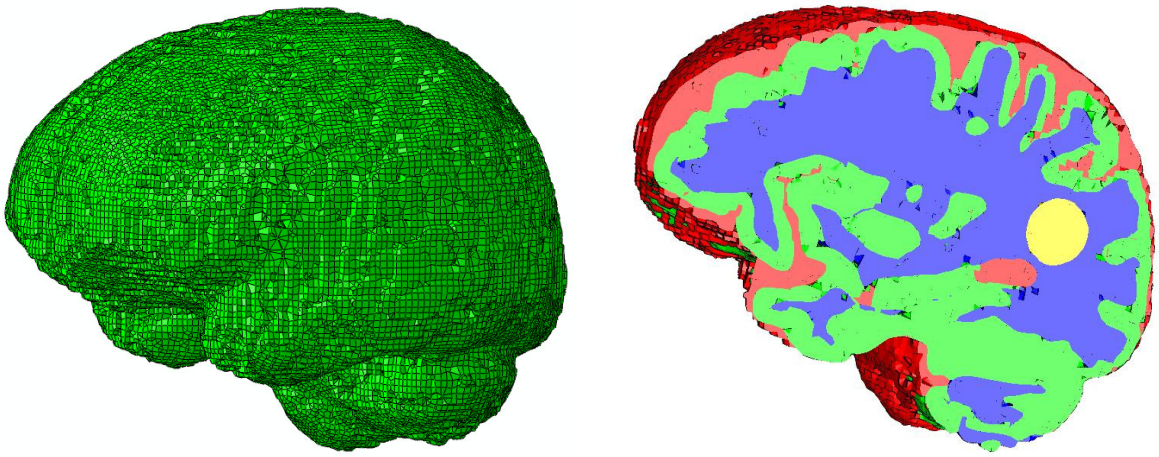

Figure 5: Finite element model of the brain used for the simulation of the tumor growth. The different colors represent the anatomical structures with distinct material properties.

The mesh generated was written in the XML format interpreted by FEBio. The algorithm used to generate the mesh associate one voxel of the image to an element in the mesh (figure 5). Therefore, in order to limit the size of the mesh, the image stack was resampled by a factor 2. The final mesh consisted of 255841 nodes and 194582 elements among which 94215 hexahedral elements and 161626 prism elements. A total of 11392 elements were removed because they had negative of null jacobians, representing 5% of the total number of elements. These elements are mostly on the external surface of the brain. This was largely due to the complex structures such as folds that appear on the surface of the brain. Because of their distance from the tumor, their removal do not have influence on the result of the simulation. The whole process (including generation of the mesh, smoothing, correction via prism division and generation of the XML file) took 3.28 minutes on a Pentium 4/2.4GHz CPU with 2GB of RAM and was fully automatic.

3.3 Material properties and boundary conditions

The material properties defined in (Clatz et al., 2005) were used (table 1). The experimental data on the mechanical properties of tumor is extremely scarce. Therefore, as suggested by (Wittek et al., 2007), it was assumed that the properties of the tumor were close to those of the surrounding soft tissue. Considering the fact that the simulation was performed for a large time, viscoelastic effects were neglected and finite elastic properties were used (table 2). Viscoelastic tissue exhibit different properties depending on the strain rate and reach equilibrium after a certain time. These effects are therefore attenuated by large time scale simulations and slow motions. The skull was not included in the model. Instead, displacement of the nodes on the external surface of the model was fully constrained.

	Young's modulus (Pa)	Poisson ratio
White matter	694	0.4
Grey matter	694	0.4
Cerebrospinal fluid	0.001	0.001
Tumor	694	0.4

Table 2: Mechanical properties used for the model of the brain. For simplification, the materials were considered as elastic.

3.4 Results of the simulation

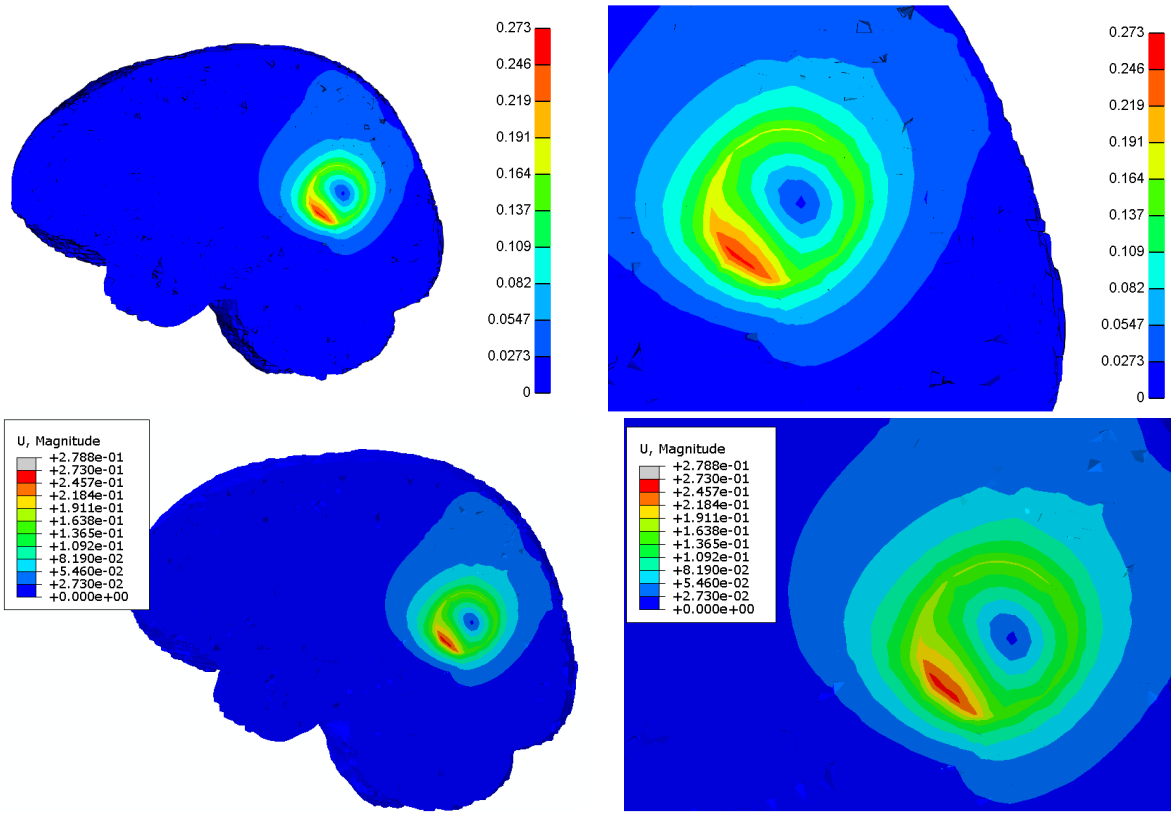

Figure 6: (top) Magnitude of displacement for the growth of a tumour in the brain as calculated by FEBio and (bottom) as calculated by the commercial software ABAQUS

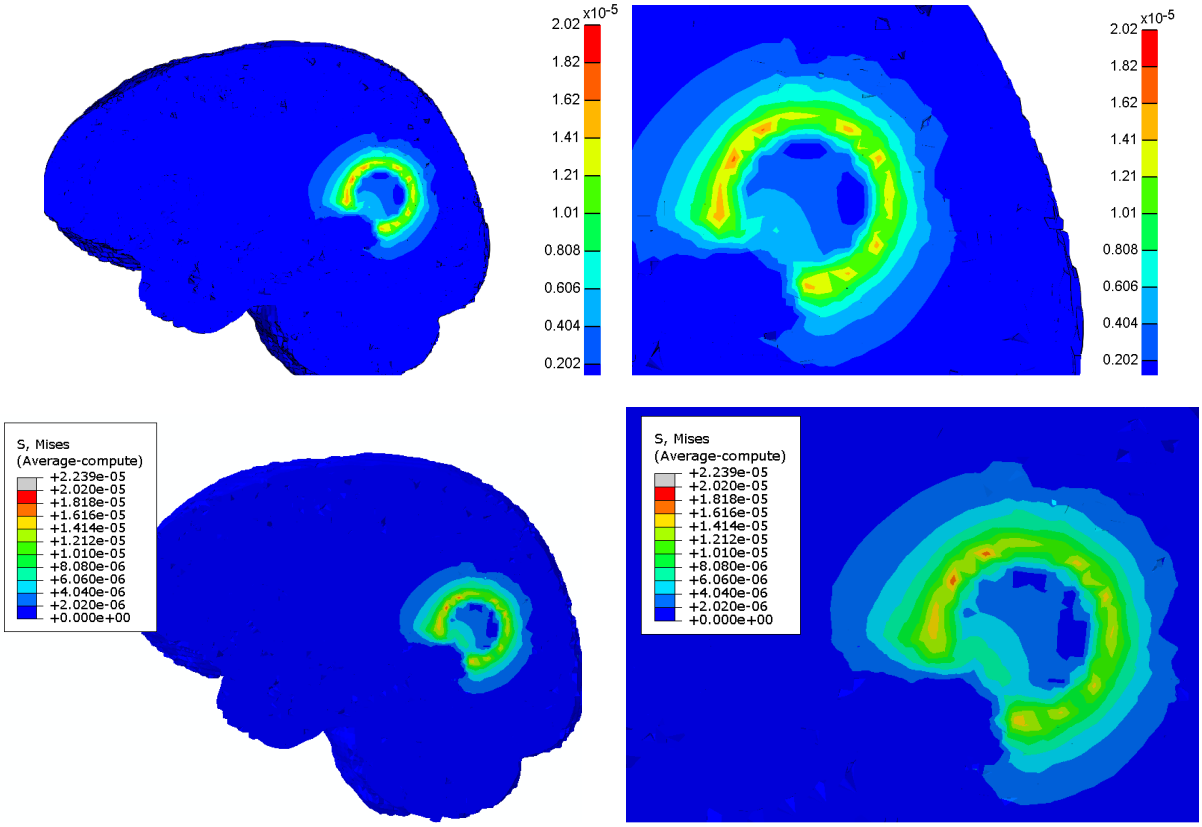

Figure 7: (top) Mises stress for the growth of a tumour in the brain as calculated by FEBio and (bottom) as calculated by the commercial software ABAQUS

Results show that the magnitude of displacement (figure 6) and Mises stresses (figure 7) are equivalent for FEBio and the commercial software ABAQUS, proving that FEBio is a valid basis for the calculation of the patient-specific stresses and strains while offering more flexibility.

4 Calculation of stresses and strains in the lung

The simulation performed for the brain was extended to a model of the lung. Again stresses and strains due to tumor mass effect were calculated using finite element analysis.

4.1 Lung images

The lung model was constructed from CT data provided and segmented in WP7 by Philips. The size of this image was 512x512x415 voxels. The original segmented mask contained more than 20 labels differentiating different areas in the lungs, vertebras and other anatomical structures. This data was simplified so to finally bear only two labels :

- The vertebra and ribs (with bone mechanical properties)
- The lungs (with soft tissue material properties)

Similarly to the brain case, the tumor was artificially added to the image stack by adding a 10mm diameter sphere to the data (figure 8).

Figure 8: (left) The lung atlas used for the generation of the model. (right) the phantom with the artificial tumour generated.

4.2 Generation of the finite element mesh

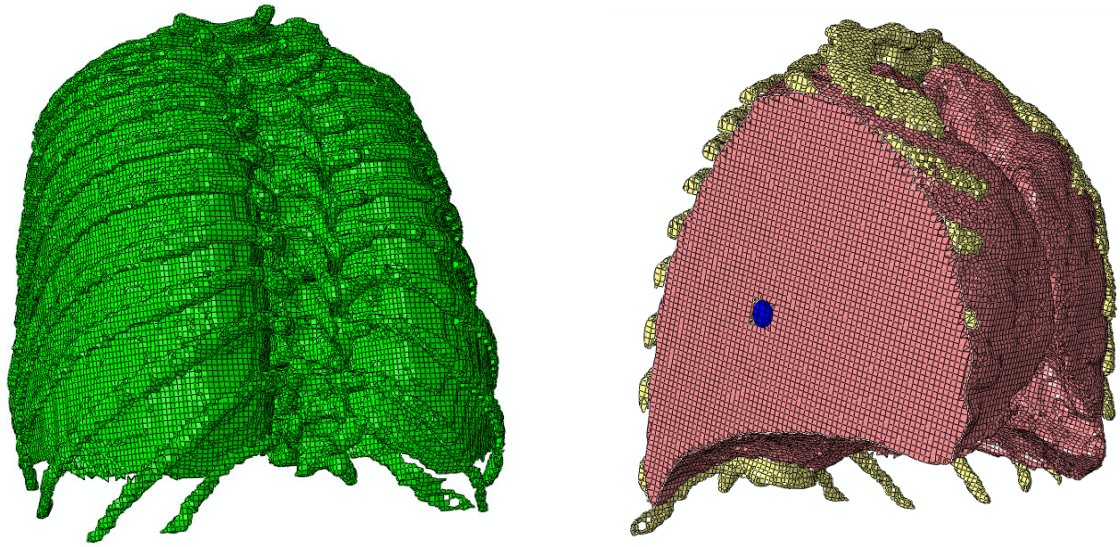

Figure 9: finite element model of the brain used for the simulation of the tumor growth. The different colors represent the different anatomical structures used for the simulation.

The same algorithm as for the brain model was used for the lung model (figure 9). This time, the image was resampled by a factor 4 to generate a model with 264128 nodes and 253356

elements among which 198469 hexahedral and 54887 prisms. Due to their negative jacobians, 1380 elements were removed from the original mesh. This number was smaller than for the brain since lungs have a more regular shape that brain surface that bears a lot of folds. The creation of the mesh took 3.95 minutes. Again, the whole process was entirely automatic.

4.3 Material properties and boundary conditions

The material properties for the soft tissue were taken from (Ganesan et al., 1995). The tissues were considered as linear elastic. Similarly to the brain model, the properties of the tumor were taken similar to the surrounding soft tissue.

	Young's modulus (Pa)	Poisson ratio
Lung tissue	961	0.4
Bone	10000E6	0.3
Tumor	961	0.4

Table 3: Mechanical properties used for the model of the lung. For simplification, the materials were considered as linear elastic.

Because of the large time over which the simulation was considered, breathing motion and heartbeat were neglected. Regarding the boundary condition, the external surface of the mesh was fully constrained.

4.4 Results of the simulation

Similarly to the brain case, the displacement and Mises stress (figure 10 and 11) due to tumor growth were calculated in the soft tissues. The uniformity of the lung tissue explain the more homogeneous results obtained as compared to the brain.

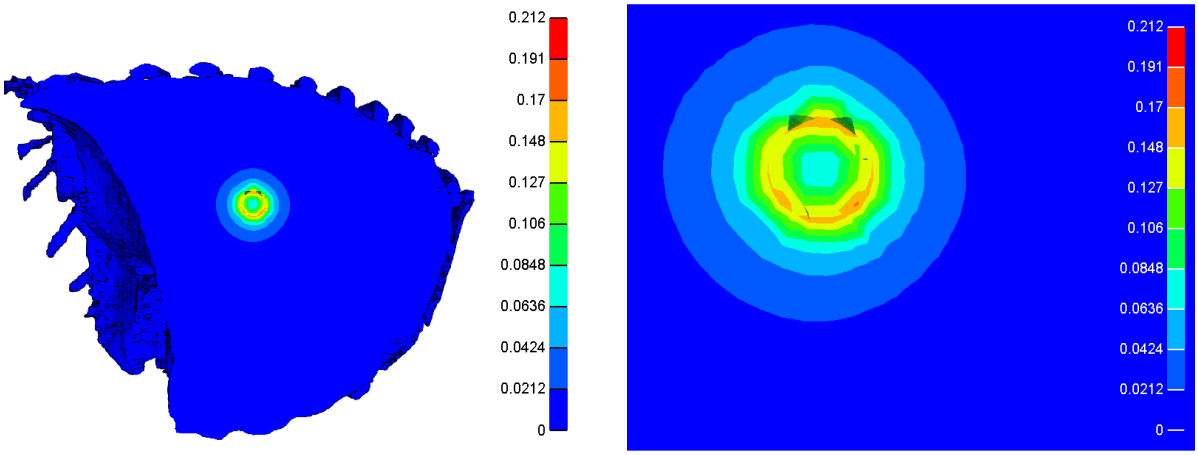

Figure 10: Magnitude of displacement for the growth of a tumour in the lung as calculated by FEBio.

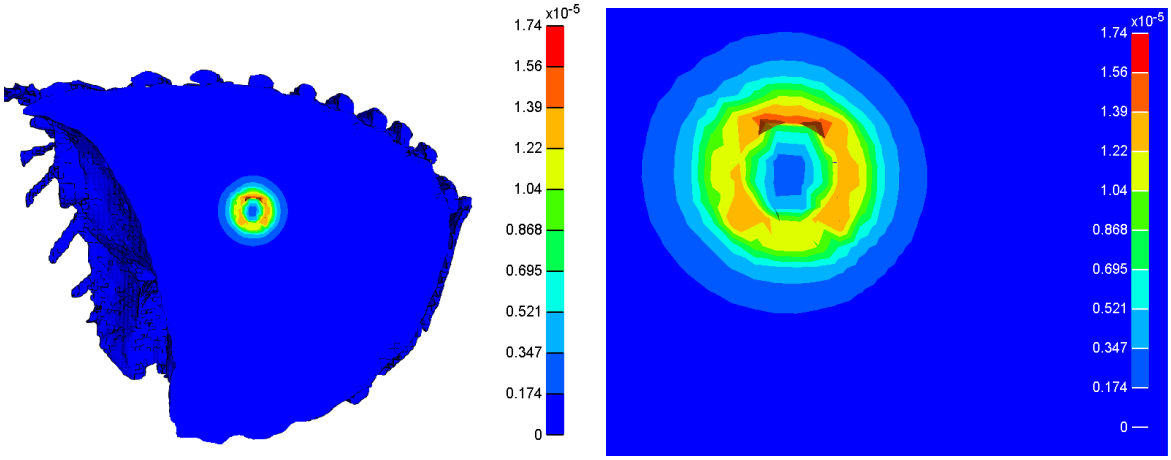

Figure 11: Mises stress for the growth of a tumour in the lung as calculated by FEBio.

5 Coupling

5.1 General principles

The coupling of diffusion/reaction and mass effect has been simulated in FEBio to further assess the capabilities of the solver. The approach used to model this coupling was similar to that of Clatz et al. (Clatz et al., 2005). The simulations were only performed in the brain where parameters could easily be recovered from previous works.

The workflow of the process was the following (figure 12). A diffusion/reaction step was used to simulate the invasion of cancerous cells in the healthy tissue. A mass effect simulation (as presented in the previous sections) was then performed to grow the elements proportionally to the quantity of cancerous cells that had been produced and diffused in each element of the mesh. The deformation of the mesh was then used to initialize a new

diffusion step. The process looped by alternating between the two simulation types. In the future the reaction/cell production part of this simulation will be provided by the cellular simulator presented in D4.1 and D4.2.
The reaction/diffusion solver was first implemented in FEBio. For the sake of validation, the diffusion simulation was tested on simple examples. The results given by the simulation were compared to the analytical equation proposed in D4.2 by Alexandros Roniotis and to other commercial finite element softwares (figure 13).
The coupling between the diffusion and mass effect was also added to the code. The two steps were solved sequentially. Information such as node displacement, cell concentration for example was transferred from one simulation to the other via vectors and was used to initialize the subsequent simulation.

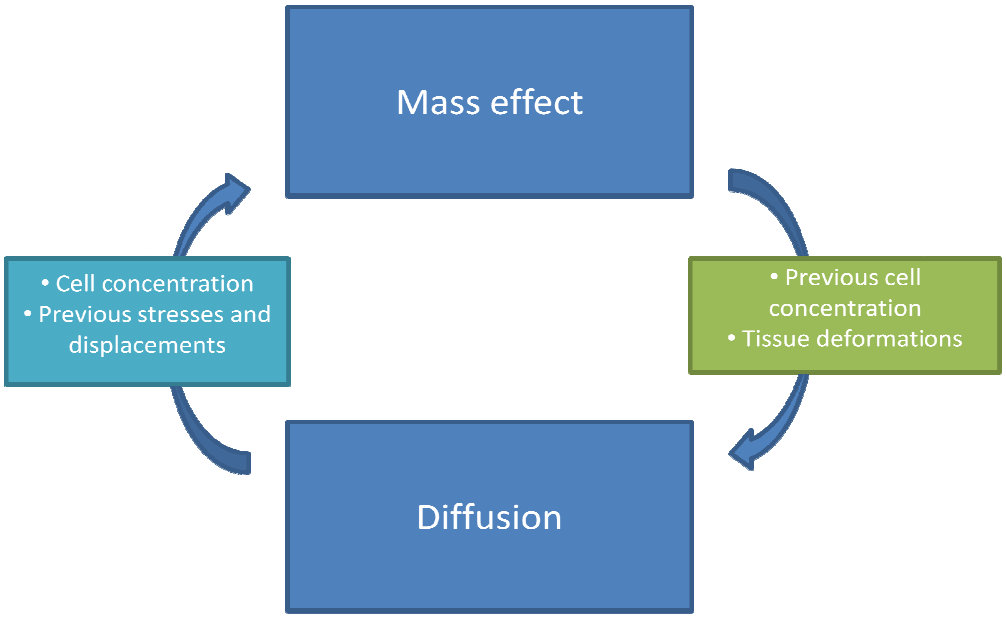

Figure 12: Flowchart of the diffusion/mass effect coupling simulation used to simulate tumor growth.

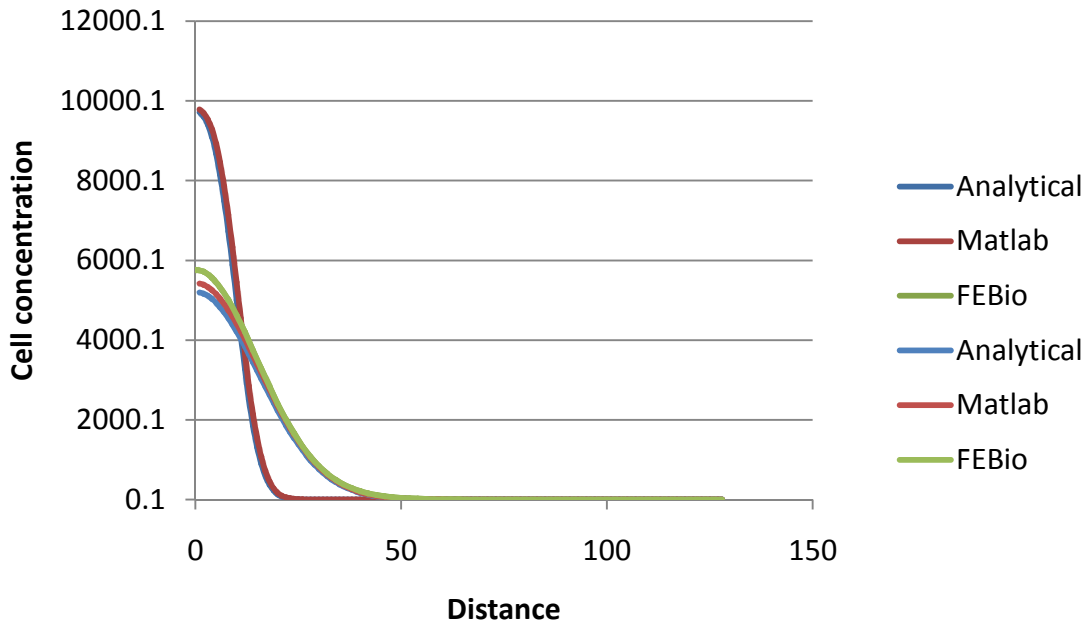

Figure 13: Comparison of the diffusion in the sphere example presented in the D4.2 as calculated by FEBio, the commercial software matlab and the analytical solution.

5.2 Model parameters

This section describes the boundary conditions and material properties used to build the model. The values proposed by Clatz et al. were mostly used for the simulation. The mesh of the brain used for the calculation was the same as the one presented in the previous sections.

5.2.1 Mass effect

The material properties of brain tissues and boundary conditions defined in section 2.3 were used. The relationship between cell concentration increase and volume change had to be defined. For sake of simplification we assumed a linear relationship defined as follow:

- If the density of cells reached or was equal to the maximum carrying capacity of the tissue (3.5e4 Cells.mm^{-3}) then a fixed growth strain is imposed to the element (a value of 2% was taken arbitrarily)
- Otherwise, the increase of volume depended linearly on the number of cancerous cells.

At each step, the displacement at every node and stress at every integration point was transmitted to the diffusion simulation.

5.2.2 Reaction/Diffusion

The diffusive part of tumor growth was simulated using the reaction diffusion law:

$$\frac{\partial c}{\partial t} = div(D_t \nabla c) + \rho c$$

Where c is the concentration of cancerous cells, D_t is the diffusion tensor indicating the preferential direction of diffusion in the tissue.
The diffusivity properties of the different tissues were defined so that the white matter diffusivity was a hundred times larger than that of the grey matter (table 4). The CSF was considered as a no diffusive material.

	Diffusivity ($10^{-3}mm^2day^{-1}$)
Grey matter	86400e-4
White matter	86400e-2
CSF	0
Skull	0

Table 4: Diffusivity properties used for the model of the brain.

The boundaries of the models were defined so that no diffusion was possible outside of the brain tissue (Neumann boundary condition). The original tumor was constrained so as to have a constant concentration of cells (3.5e4 $Cells.mm^{-3}$). The tumor was considered as a one component object. The difference in behavior between the GTV1 and GTV2 zone was neglected.
The source parameter ρ representing the production of cancerous cells per day was set to 2.2e-5day^{-1}.

Results

The calculations were performed for a time period of six months (figure 14). The results showed that growth primarily occurred in tissues where the diffusivity was higher (white matter) and in the tumor. The structures in white matter were obviously enlarged after the simulation time. The lack of diffusion in the CSF and the grey matter was clearly visible on the colormap plots. The large span of cancerous cells in the brain tissue proved that the diffusion component has to be considered for the simulation of the growth of the tumor.
These promising results will lead in the next steps to a more advanced model with more clinical information. One of the possible additions is the diffusivity tensor of tissues retrieved for DT MRI in the diffusion equation. The invasion of the cancerous cells was here fully isotropic which explains the relatively circular growth of the tumor.

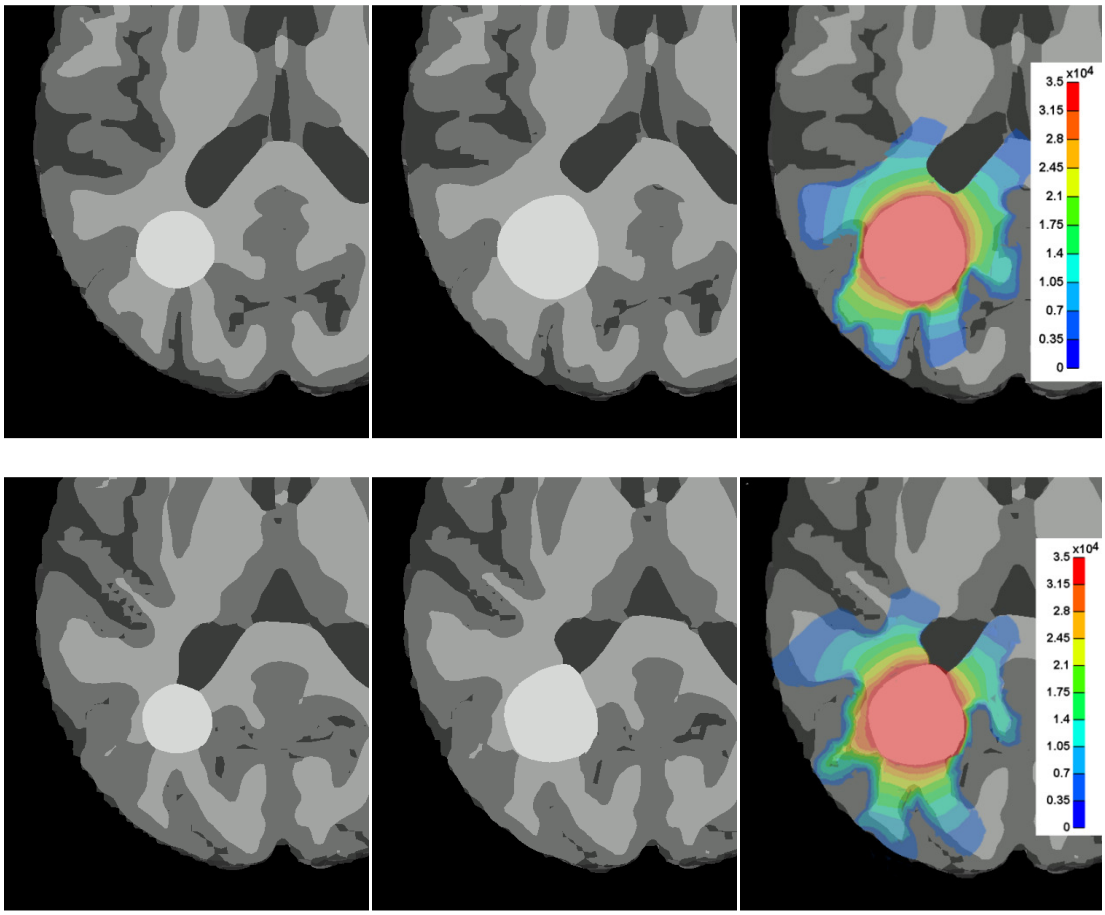

Figure 14: Result of the couple growth for different slices of the brain MRI (top and bottom). From left to right, original configuration of the brain, deformed configuration of the brain showing the mass effect of tumor growth, result of the reaction/diffusion simulation mapped onto the deformed model.

6 Conclusions

The aim of this deliverable was to provide the tools for stress and strain calculations in the brain and lung under tumor growth using the finite element method. This section presents a short overview of the work that has been done to achieve this goal and gives a few directions for future work.

6.1 Contributions

This part of the project offers several challenges. One of them is the fact that the finite element tool chosen for the project does not originally include the different tools used to simulate tumor growth. A large part of the effort has then been focused on modifying the existing code and implementing these missing elements. In a first section, a material law that takes into account the mass effect of growth has been added to the finite element code. It

has been tested successfully on both brain and lung models and provide stresses and strains in the tumor and surrounding tissues. Both models were created fully automatically by the custom meshing algorithm, which guarantees easy integration of the process in the clinical flow that is aimed by ContraCancrum.
In the next section, a reaction/diffusion law was added so as to include this important physiological parameter in the simulation. The mass effect law and diffusion/reaction model were combined and coupled to simulate a more realistic growth of the tumor. Results show selected growth of the tumor in tissues where diffusivity is higher. This simplified model proves the feasibility of this type of analysis and is ready to be integrated in the general oncosimulator.

6.2 Future work

- The main direction to be taken will be the combination of the cellular simulator with the biomechanical model shown in the present document. Cell production will be fed into the mass effect model coupled with diffusion. The new concentration of cells, stresses, strains and deformation brought back to the cellular level.
- The results of the model are for the moment simplified and further discussion with partners from the University of Athens and clinicians will help define the missing parameters. Among possible improvements to the model stands the preconstraint in the surrounding tissue due to the tumor, pressure exerted by CSF around the brain and in the ventricles.
- The implementation of the coupling can be improved and accelerated by combining the stiffness matrix and the diffusion matrix into one that will be solved in one step. This way, the two part of the coupling can be solved simultaneously instead of sequentially.
- Results provided by in the D4.1 show that diffusion as calculated with the finite difference gives faster results. A collaborative work will be done with partners from FORTH to investigate what would be the most optimal combination between different simulators. This would also provide the benefit of the coupling approach to the Oncosimulator.
- Large deformations due to excessive growth may generate for some cases low quality elements which prevent the solution of the problem. Several methods are currently investigated and implemented to solve this problem. The first solution consists in remeshing the model after some simulation steps. This method has given positive results in previous works. An alternative is the use of Eulerian finite element models usually used in flow simulation. In these models, the mesh is considered as fixed and the simulation calculates the “flow of material” through this fixed mesh.

Reference List

Al Mayah, A., Moseley, J., Velec, M. & Brock, K.K. (2009) Sliding characteristic and material compressibility of human lung: parametric study and verification. *Med.Phys.* **36:** 4625-4633.

Bates, J.H. (1993) Understanding lung tissue mechanics in terms of mathematical models. *Monaldi Arch.Chest Dis.* **48:** 134-139.

Carter, T.J., Sermesant, M., Cash, D.M., Barratt, D.C., Tanner, C. & Hawkes, D.J. (2005) Application of soft tissue modelling to image-guided surgery. *Med.Eng Phys.* **27:** 893-909.

Chakrabarty, S.P. & Hanson, F.B. (2009) Distributed parameters deterministic model for treatment of brain tumors using Galerkin finite element method. *Math.Biosci.* **219:** 129-141.

Clatz,O., Bondiau,P.Y., Delingette,H., Sermesant,M., Warfield,S.K., Malandain,G., and Ayache,N. Brain tumor growth simulation. 2004.
Ref Type: Report

Clatz, O., Sermesant, M., Bondiau, P.Y., Delingette, H., Warfield, S.K., Malandain, G. & Ayache, N. (2005) Realistic simulation of the 3-D growth of brain tumors in MR images coupling diffusion with biomechanical deformation. *IEEE Trans.Med.Imaging* **24:** 1334-1346.

Cookson, M.J., Davies, C.J., Entwistle, A. & Whimster, W.F. (1993) The microanatomy of the alveolar duct of the human lung imaged by confocal microscopy and visualised with computer-based 3D reconstruction. *Comput.Med.Imaging Graph.* **17:** 201-210.

Ganesan, S., Rouch, K.E. & Lai-Fook, S.J. (1995) A finite element analysis of the effects of the abdomen on regional lung expansion. *Respir.Physiol* **99:** 341-353.

Juffer, A.H., Marin, U., Niemitalo, O. & Koivukangas, J. (2008) Computer modeling of brain tumor growth. *Mini.Rev.Med.Chem.* **8:** 1494-1506.

Konukoglu, E., Sermesant, M., Clatz, O., Peyrat, J.M., Delingette, H. & Ayache, N. (2007) A recursive anisotropic fast marching approach to reaction diffusion equation: application to tumor growth modeling. *Inf.Process Med.Imaging* **20:** 687-699.

Maas,S.A., Ellis,B.J., Rawlins,D.S., and Weiss,J.A. A comparison of FEBio, ABAQUS, and NIKE3D. Results for a suite of verification problems. UUSCI-2009-009. 2009. Scientific Computing and Imaging Institute, University of Utah, Salt Lake City, UT 84112 USA.

Ref Type: Report

Miller, K. (1999) Constitutive model of brain tissue suitable for finite element analysis of surgical procedures. *J.Biomech.* **32:** 531-537.

Mohamed, A. & Davatzikos, C. (2005) Finite element modeling of brain tumor mass-effect from 3D medical images. *Med.Image Comput.Comput.Assist.Interv.* **8:** 400-408.

Murray,J.D. (2003) *Mathematical Biology. II: Spatial models and biomedical applications*. Springer, New York, NY.

Raul, J.S., Deck, C., Willinger, R. & Ludes, B. (2008) Finite-element models of the human head and their applications in forensic practice. *Int.J.Legal Med.* **122:** 359-366.

Rohlfing, T., Zahr, N.M., Sullivan, E.V. & Pfefferbaum, A. (2010) The SRI24 multichannel atlas of normal adult human brain structure. *Hum.Brain Mapp.* **31:** 798-819.

Sundaram, T.A. & Gee, J.C. (2005) Towards a model of lung biomechanics: pulmonary kinematics via registration of serial lung images. *Med.Image Anal.* **9:** 524-537.

Swanson,K.R. (1999) Mathematical modeling of tumor growth and control of tumors. University of Washington.

Tawhai, M.H., Nash, M.P., Lin, C.L. & Hoffman, E.A. (2009) Supine and prone differences in regional lung density and pleural pressure gradients in the human lung with constant shape. *J.Appl.Physiol* **107:** 912-920.

Taylor, Z. & Miller, K. (2004) Reassessment of brain elasticity for analysis of biomechanisms of hydrocephalus. *J.Biomech.* **37:** 1263-1269.

van Ertbruggen, C., Hirsch, C. & Paiva, M. (2005) Anatomically based three-dimensional model of airways to simulate flow and particle transport using computational fluid dynamics. *J.Appl.Physiol* **98:** 970-980.

Voo, K., Kumaresan, S., Pintar, F.A., Yoganandan, N. & Sances, A., Jr. (1996) Finite-element models of the human head. *Med.Biol.Eng Comput.* **34:** 375-381.

Wasserman, R. & Acharya, R. (1996) A patient-specific in vivo tumor model. *Math.Biosci.* **136:** 111-140.

Wittek, A., Miller, K., Kikinis, R. & Warfield, S.K. (2007) Patient-specific model of brain deformation: application to medical image registration. *J.Biomech.* **40:** 919-929.

Zeng, Y.J., Yager, D. & Fung, Y.C. (1987) Measurement of the mechanical properties of the human lung tissue. *J.Biomech.Eng* **109:** 169-174.